ChemComm

RSC Publishing

COMMUNICATION

View Article Online
View Journal | View Issue

Separately doped upconversion-C_{60} nanoplatform for NIR imaging-guided photodynamic therapy of cancer cells†

Cite this: *Chem. Commun.*, 2013, **49**, 3224

Received 6th February 2013,
Accepted 1st March 2013

DOI: 10.1039/c3cc41013g

www.rsc.org/chemcomm

Xiaomin Liu,[a] Min Zheng,[a] Xianggui Kong,*[a] Youlin Zhang,[a] Qinghui Zeng,[a] Zaicheng Sun,[a] Wybren Jan Buma[b] and Hong Zhang*[b]

A highly efficient upconversion-C_{60} nanoplatform was demonstrated for NIR imaging-guided photodynamic therapy of cancer.

Lanthanide ion (Ln^{3+}, such as Er^{3+}, Tm^{3+}, Ho^{3+})-doped upconversion nanoparticles (UCNPs) are emerging as a new generation of multimodal bioprobes, and have attracted a large interest for a variety of biological applications.[1,2] The developed luminescent UCNP based photosensitizing nanoplatforms,[3] which can be excited with NIR light (~980 nm) falling in the biological window of tissues and generating multicolour emission in the visible spectral region,[4] have made image-guided photodynamic therapy (PDT) possible. $^1O_2$ is generated in these cases through photosensitizers (PSs) that are activated by energy transfer from UCNPs upon NIR excitation. However, most UCNP-based PDT applications have been limited by the relatively low $^1O_2$ production yield. Several strategies have been employed to improve the performance of such nanoplatforms, *e.g.* developing a covalent strategy to shorten the energy transfer distance,[5] using a combination of two PSs for optimally utilizing the upconversion luminescence.[6] However, the majority of the currently used PSs are aromatic molecules that have negative side effects and do not have a very high $^1O_2$ yield. Searching for more efficient therapeutic agents has led numerous groups to investigate the potential of fullerene derivatives as novel PDT drugs.[7] Such molecules are particularly attractive because of their broad absorption spectra,[8] lack of dark toxicity and high quantum yield to form reactive species (100% based on generation of $^1O_2$).[9,10]

In this work, we present a NIR-triggered NIR imaging-guided PDT nanoplatform based on multiplexed Förster resonance energy transfer (FRET) in which multicolour UCNPs are used as donors and monomalonic fullerene (C_{60}MA) as an acceptor. They are an ideal donor–acceptor pair. Upon 980 nm CW light excitation, upconversion luminescence (UCL) of a $NaYF_4$:Yb^{3+},Er^{3+}/$NaYF_4$:Yb^{3+},Tm^{3+} separately doped nanostructure appears simultaneously around 450, 475, 540, 650 and 808 nm. All of these bands, except the 808 nm band, contribute to the transfer of excitation energy to C_{60}MA due to the broad absorption band of the latter and thus trigger PDT. At the same time, the 808 nm emission can be used for high-contrast NIR luminescence imaging as illustrated in Fig. 1. *In vitro* experiments on cancer cells verify the efficient photodynamic effects of the nanoplatform. As the first demonstration of a multifunctional UCNP–fullerene nanoplatform, this result offers a new possibility in exploring highly stable and efficient nanoplatforms suitable for NIR imaging-guided therapy of cancers.

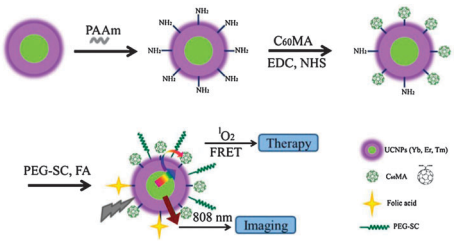

Fig. 1 The construction and operating principle of the nanoplatform.

In order to generate strong multicolour upconversion luminescence, oleylamine-coated $NaYF_4$:Yb^{3+},Er^{3+}/$NaYF_4$:Yb^{3+},Tm^{3+} separately doped UCNPs were synthesized following a previously reported protocol (see ESI†). The composition, phase purity and morphology of these nanoparticles were examined by TEM and XRD as shown in Fig. 2a (see also Fig. S1–S3, ESI†). From the TEM images it could be concluded that the UCNPs have a good monodispersity with an average diameter of about 45 nm. We employed a strategy of separately doping core and shell with Er^{3+} and Tm^{3+} instead of homogeneous co-doping to achieve strong multicolour upconversion luminescence (Fig. S4, ESI†).[11]

Hydrophilic NH_2-functionalized UCNPs were prepared following a ligand exchange process using poly(allylamine) as a surface-coating agent. Phase transfer caused negligible effect on the UCL spectrum (Fig. S5, ESI†). To optimize the energy transfer distance and ensure that the majority of C_{60}MA

[a] *State Key Laboratory of Luminescence and Applications, Changchun Institute of Optics, Fine Mechanics and Physics, Chinese Academy of Sciences, China. E-mail: xgkong14@ciomp.ac.cn*
[b] *Van't Hoff Institute for Molecular Sciences, University of Amsterdam, The Netherlands. E-mail: h.zhang@uva.nl*

† Electronic supplementary information (ESI) available: Characterization of samples and experimental procedure. See DOI: 10.1039/c3cc41013g

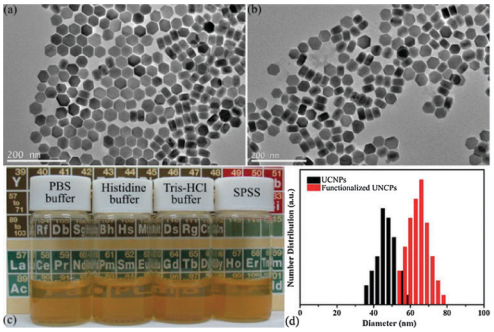

Fig. 2 (a) TEM image of separately doped $NaYF_4$:Yb^{3+},Er^{3+}/$NaYF_4$:Yb^{3+},Tm^{3+} UCNPs. (b) TEM image of UCNP–C_{60}MA nanoconjugates. (c) Photos of the UCNP–C_{60}MA nanoconjugates dispersed in various biological media (SPSS: stroke-physiological saline solution). (d) Hydrodynamic diameter distributions of the UCNPs before and after surface functionalization.

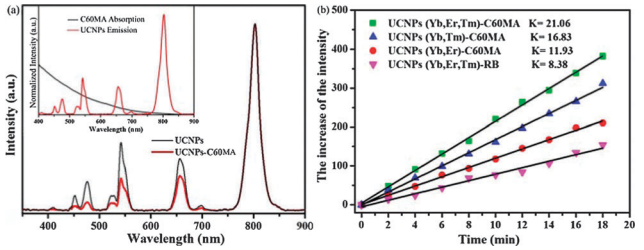

Fig. 3 (a) UCL spectra of UCNPs and UCNP–C_{60}MA (normalized by the intensity at 808 nm). Insert: spectral overlap between the emission of the donor UCNPs (red) and the absorption of the acceptor C_{60}MA (black). (b) The increase in luminescence intensity of FCLA at 524 nm as a function of the exposure time under 980 nm irradiation.

molecules were firmly linked to UCNPs, a covalent conjugation strategy was followed that involved a crosslinking reaction between the amino group of the UCNPs and the carboxyl group of C_{60}MA. For the sake of solving the low dispersity of fullerenes in biologically relevant media,[12] PEG-succinimidyl carbonate (PEG-SC), which has a good compatibility with biological systems and can reduce the undesired toxicity of nanoparticles, was used to stabilize the nanocomposites in various biological solvents (Fig. 2c). The conjugation with C_{60}MA did not alter the size and morphology of the UCNPs (Fig. 2b). Fig. 2d shows that the effective hydrodynamic diameter distributions of the UCNPs before and after conjugation were centered at 46 nm and 64 nm, respectively, indicating successful functionalization. Covalent coupling between UCNPs and C_{60}MA was confirmed from FTIR absorption spectra shown in Fig. S6 (ESI†). After conjugation with UCNPs, the peak at 1717 cm^{-1} (C=O stretching mode of the carboxyl group on C_{60}MA) disappeared and two new peaks associated with the C=O stretching and N–H bending modes of a secondary amide appeared at 1648 and 1556 cm^{-1}, respectively. The observation of a dark brown precipitate and a nearly colourless supernatant after centrifugation—while no precipitate or colour change was noticed in the bare C_{60}MA sample—further confirmed the bonding of C_{60}MA (Fig. S7, ESI†). The C_{60}MA loading capacity was characterized using UV-VIS spectroscopy. The absorption of UCNP–C_{60}MA composites became larger with increasing amounts of C_{60}MA and saturated at 10.5% (w/w) at C_{60}MA concentrations above 300 μL (0.25 mg mL^{-1}) (Fig. S8, ESI†).

The present multifunctional nanoplatform was constructed guided by the fact that the broad absorption spectrum of C_{60}MA overlaps well with the multicolour upconversion luminescence bands (450, 475, 540, 650 nm) of $NaYF_4$:Yb^{3+},Er^{3+}/$NaYF_4$:Yb^{3+},Tm^{3+} (inset of Fig. 3a). Energy transfer from UCNPs to C_{60}MA was confirmed from both steady-state UCL spectra and the luminescence decay kinetics. The UCL spectra in Fig. 3a demonstrate that the 450, 475, 540 and 650 nm bands were significantly quenched by C_{60}MA. The FRET efficiency was determined from the quenching of UCL as $E = (I_0 - I_1)/I_0$, where I_0 and I_1 are the emission intensities of UCNPs and UCNP–C_{60}MA nanoconjugates, respectively,[13] leading to efficiencies of 79% at 450 nm, 72% at 475 nm, 61% at 540 nm, and 45% at 650 nm. We attribute the high energy transfer efficiency partly to the robust covalent binding between C_{60}MA and UCNPs. The energy transfer process was further verified by the temporal behavior of UCL of both UCNPs and UCNP–C_{60}MA composites recorded at 450, 475, 540 and 650 nm (Fig. S9, ESI†). The significant shortening of the upconversion luminescence kinetics that was observed in these experiments is in line with the strong energy transfer concluded from the analysis of the steady-state UC luminescence quenching.

Another aspect entering the design of our UCNP–C_{60}MA nanoplatform is the high $^1O_2$ production yield of C_{60} derivatives, which is even higher than those of traditional photosensitizers such as rose bengal, methylene blue and eosin yellowish.[14] In order to assess the capability of our UCNP–C_{60}MA nanoplatform to generate $^1O_2$, we employed the chemiluminescence of a fluoresceinyl Cypridina luciferin analogue (FCLA). FCLA can be oxidized by $^1O_2$, resulting in an increase of its fluorescence at around 524 nm, and can thus be used as a $^1O_2$ detector.[15] Fig. S11a (ESI†) illustrates the FCLA fluorescence intensity variation in the presence of UCNP–C_{60}MA nanocomposites. Without the nanocomposites or 980 nm light illumination, the FCLA luminescence showed a negligible change with time (Fig. S10, ESI†). When illuminated with 980 nm light, the fluorescence of FCLA in UCNP–C_{60}MA solutions was boosted, indicating efficient generation of $^1O_2$. To further illustrate that our nanoplatform is indeed superior, three other energy transfer models, *i.e.*, (i) UCNPs (Yb, Er)–C_{60}MA, (ii) UCNPs (Yb, Tm)–C_{60}MA and (iii) UCNPs (Yb, Er, Tm)–rose bengal were constructed. Fluorescence spectra of FCLA, recorded as a function of exposure time under 980 nm irradiation are shown in Fig. S11 (ESI†) for these three samples and the UCNP (Yb, Er, Tm)–C_{60}MA samples. The corresponding fluorescence intensity changes are depicted in Fig. 3b. Since the slopes of the curves represent the efficiency of singlet oxygen generation, it is clear that the designed UCNP (Yb, Er, Tm)–C_{60}MA nanocomposites are indeed a highly efficient nanoplatform for $^1O_2$ generation and potentially for NIR light triggered photodynamic therapy of cancer.

We studied the cellular uptake of UCNP–C_{60}MA by HeLa cells. To this purpose, the targeting molecule, folic acid (FA), was covalently linked to UCNP–C_{60}MA. Fig. 4a shows the target staining of the UCNP–C_{60}MA/FA nanoplatform in HeLa cells and the control result using human alveolar adenocarcinoma (A549) cells. The upconversion luminescence was collected at

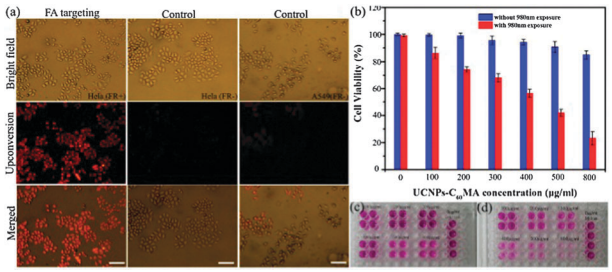

Fig. 4 (a) Specificity of the UCNP–C_{60}MA nanoconjugates. HeLa cells were cultured in folate-free medium (left, positive) and in folate-supplemented medium (middle, negative). A negative control was also performed with A549 cells (right). Scale bar, 50 μm. (b) Cell viability of HeLa cells treated with UCNP–C_{60}MA of different concentration with or without 980 nm exposure. (c and d) Photographs of purple formazan dissolved in DMSO, indicating the viability of cells treated with nanoconjugates without (c) and with (d) 980 nm exposure.

808 nm, a wavelength that lies in the biological window (700–1100 nm) and enables high-contrast optical imaging.[16] The nanocomposites were mainly located within the cells (Fig. 4a, left), illustrating the specific targeting of the nanoplatform. The absence of autofluorescence confirmed that the UCNP–C_{60}MA/FA platform can be used for high-contrast luminescence imaging of cells *in vitro*. When the folate receptors on the cancer cell membranes were saturated by free folic acid before incubating with the nanoplatform, just a few UCNP–C_{60}MA/FA nanoconjugates were stained in the cancer cells (Fig. 4a, middle), which might be due to the nonspecific adsorption of UCNPs. Furthermore, there was no significant morphology change of the cancer cells in the bright field image (Fig. 4a, top), suggesting a good biocompatibility of the nanoplatform. To further verify the specificity of the UCNP–C_{60}MA/FA composites, A549 cells, which are poor in expressing the folate receptor, were used for a negative control (Fig. 4a, right). In this case only a few UCNPs were observed in the cells.

The photodynamic capabilities of the UCNP–C_{60}MA nanoplatform were studied by incubating HeLa cells with UCNP–C_{60}MA at different concentrations. The cell viabilities, as determined by 3-(4,5-dimethythiazol-2-yl)-2,5-diphenyltetrazolium bromide (MTT) assay, are shown in Fig. 4b. MTT can be reduced to purple formazan in living cells. DMSO solution was added to dissolve the insoluble purple formazan product. The absorbance of this coloured solution was roughly proportional to the number of living cells (Fig. 4c and d). Dark toxicity was also evaluated. No significant decrease in viability was observed in the control test. The toxicity became only non-negligible when the concentration was higher than 800 μg mL^{-1} (100 μL), suggesting that the nanocomposites have a low inherent concentration-dependent toxicity (Fig. 4b and c). When HeLa cells were exposed to NIR light at a relatively low intensity of 1.37 W cm^{-2}, the cells declined rapidly with an increase in the concentration of UCNP–C_{60}MA nanocomposites (Fig. 4b and d), indicating the efficiency in killing cancer cells *via* PDT. To further prove the PDT efficiency of the UCNP–C_{60}MA nanoplatform, the photodynamic capabilities of the other three energy transfer models were also tested for comparison (Fig. S13, ESI†). It can be concluded that the reduction in viability was the most in cells treated with UCNP (Yb, Er, Tm)–C_{60}MA, emphasizing the superiority of the designed photosensitizing nanoplatform.

This work was financially supported by the NSF of China (11004189, 11174277, 61275202 and 61275197), a joint research program between CAS of China and KNAW of the Netherlands, the IOP program of The Netherlands, and John van Geuns foundation. Z.S. thanks the ''Hundred Talent Program of CAS'' for support.

Notes and references

1 J. P. Celli, B. Q. Spring, I. Rizvi, C. L. Evans, K. S. Samkoe, S. Verma, B. W. Pogue and T. Hasan, *Chem. Rev.*, 2010, **110**, 2795.
2 (*a*) Y. S. Liu, S. Y. Zhou, D. T. Tu, Z. Chen, M. D. Huang, H. M. Zhu and X. Y. Chen, *J. Am. Chem. Soc.*, 2012, **134**, 15083; (*b*) J. L. Liu, Y. Liu, Q. Liu, C. Y. Li, L. N. Sun and F. Y. Li, *J. Am. Chem. Soc.*, 2011, **133**, 15276; (*c*) N. Bogdan, F. Vetrone, G. A. Ozin and J. A. Capobianco, *Nano Lett.*, 2011, **11**, 835; (*d*) Y. L. Liu, K. L. Ai, J. H. Liu, Q. H. Yuan, Y. Y. He and L. H. Lu, *Angew. Chem., Int. Ed.*, 2012, **51**, 1437.
3 (*a*) C. Wang, H. Q. Tao, L. Cheng and Z. Liu, *Biomaterials*, 2011, **32**, 6145; (*b*) M. E. Lim, Y. L. Lee, Y. Zhang and J. J. H. Chu, *Biomaterials*, 2012, **33**, 1912; (*c*) Q. B. Xiao, Y. T. Ji, Z. H. Xiao, Y. Zhang, H. Z. Lin and Q. B. Wang, *Chem. Commun.*, 2013, **49**, 1527.
4 (*a*) F. Wang and X. G. Liu, *J. Am. Chem. Soc.*, 2008, **130**, 5642; (*b*) R. Komban, J. P. Klare, B. Voss, J. Nordmann, H. J. Steinhoff and M. Haase, *Angew. Chem., Int. Ed.*, 2012, **51**, 6506.
5 K. Liu, X. M. Liu, Q. H. Zeng, Y. L. Zhang, L. P. Tu, T. Liu, X. G. Kong, S. A. G. Lambrechts, M. C. G. Aalders and H. Zhang, *ACS Nano*, 2012, **6**, 4054.
6 N. M. Idris, M. K. Gnanasammandhan, J. Zhang, P. C. Ho, R. Mahendran and Y. Zhang, *Nat. Med.*, 2012, **18**, 1580.
7 D. M. Guldi and M. Prato, *Acc. Chem. Res.*, 2000, **33**, 695.
8 S. Fukuzumi, T. Suenobu, M. Patz, T. Hirasaka, S. Ito, M. Fujitsuka and O. Ito, *J. Am. Chem. Soc.*, 1998, **120**, 8060.
9 J. W. Arbogast and C. S. Foote, *J. Am. Chem. Soc.*, 1991, **113**, 8886.
10 T. Nagano, K. Arakane, A. Ryu, T. Masunaga, K. Shinmoto, S. Mashiko and M. Hirobe, *Chem. Pharm. Bull.*, 1994, **42**, 2291.
11 X. M. liu, X. G. Kong, Y. L. Zhang, L. P. Tu, Y. Wang, Q. H. Zeng, C. G. Li, Z. Shi and H. Zhang, *Chem. Commun.*, 2011, **47**, 11957.
12 R. S. Ruoff, D. S. Tse, R. Malhotra and D. C. Lorents, *J. Phys. Chem.*, 1993, **97**, 3379.
13 Y. Wang, K. Liu, X. M. Liu, K. Dohnalova, T. Gregorkiewicz, X. G. Kong, M. C. G. Aalders, W. J. Buma and H. Zhang, *J. Phys. Chem. Lett.*, 2011, **2**, 2083.
14 T. Hamano, K. Okuda, T. Mashino, M. Hirobe, K. Arakane, A. Ryu, S. Mashiko and T. Nagano, *Chem. Commun.*, 1997, 21.
15 A. G. Zhou, Y. C. Wei, B. Y. Wu, Q. Chen and D. Xing, *Mol. Pharmaceutics*, 2012, **9**, 1580.
16 M. Nyk, R. Kumar, T. Y. Ohulchanskyy, E. J. Bergey and P. N. Prasad, *Nano Lett.*, 2008, **8**, 3834.

